International Journal of Modern Physics B
Vol. 24, No. 4 (2010) 515–536

DOI: 10.1142/S0217979210054774

World Scientific
www.worldscientific.com

SLOW ACOUSTIC WAVES WITH THE ANTI-PLANE POLARIZATION IN LAYERED SYSTEMS

A. A. ZAKHARENKO

International Institute of Zakharenko Waves,
660037, Krasnoyarsk-37, 17701 Krasnoyarsk, Russia
aazaaz@inbox.ru

Received 10 February 2009

This paper theoretically investigates the three-partial slow surface Zakharenko-type waves (SSZTW3) with the anti-plane polarization possessing single mode and propagating in layer-on-substrate systems. The dispersive SSZTW3 can exist with the conditions on both the shear elastic constants $C_{44}^L > C_{44}^S$ and the bulk shear wave velocities $V_t^L < V_t^S$, where the superscripts L and S belong to the layer and substrate, respectively. The SSZTW3 mode starts with zero-phase velocity and approaches the maximum velocity $V_{tm} < V_t^L$ for infinite layer thicknesses. The SSZTW3 phase and group velocities were calculated for many layered structures with $V_{tm} < 1000$ m/s, for example, for Au/Paratellurite structure, where the Paratellurite is a common acousto-optic crystal. The velocities' first and higher derivatives were also obtained in order to better understand their behavior for different applications in SAW filters and sensors. The calculations of derivatives were carried out for the Au/Ftorapatite structure with the smallest value of $V_{tm} \sim 210$ m/s that is lower than any known acoustic wave velocity in tough materials. It is thought that SSZTW3 usage in MEMS-(CMUTs) technical devices can simplify technological processes. The effective masses were also calculated for different layered structures in the limit of zero-phase velocity V_{ph}, where the dispersion relations correspond to those for free quasi-particles in a vacuum. It was found that the masses are smaller than the mass of a free electron. Hence, it is expected that the SSZTW3 appearance with $V_{ph} \to 0$ can be caused by electrons.

Keywords: Interfacial slow waves; anti-plane polarization; soliton-like phonons; quasi-particle mass; phase and group velocities and their derivatives.

PACS numbers: 51.40.+p, 62.65.+k, 68.35.Gy, 68.35.Iv, 68.60.Bs, 74.25.Ld

1. Introduction

Types of surface acoustic waves (SAWs) differ from each other by their own unique features. It is thought that the most important SAW feature is the wave polarization in addition to system geometry, in which surface waves can propagate. It is well known that the Love waves[1] represent the simplest SAW example propagating in waveguides consisting of a layer on a substrate (see Fig. 1). The Love-type waves (LTW) are characterized by polarization along the x_2-axis perpendicular to the

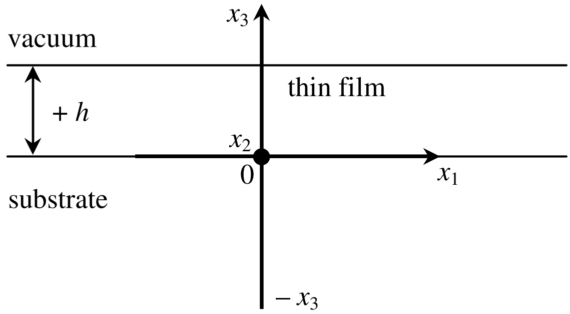

Fig. 1. The wave propagation direction in the layered system consisting of a layer on a substrate, where the x_2-axis is perpendicular to the figure plane.

sagittal plane formed by both the x_1- and x_3-axes. The LTWs can propagate in the waveguides with the existence condition: the bulk shear wave velocity V_t^S in the substrate should be higher than the velocity V_t^L in the layer. That results in all imaginary/complex wavevector components $k_3^{(n)} = k_0^{(n)} - j\chi_3^{(n)}$ along the x_3-axis negative values in the substrate for such SAW existence, $j = (-1)^{1/2}$. Therefore, the damping wave numbers $\chi_3^{(n)}$ should be positive for the LTWs; n is an integer. Note that some wave numbers along the x_3-axis in the layer should be real. That is obligatory to give an infinite number of LTW modes.

The same negative sign for the damping wave numbers $\chi_3^{(n)}$ should be taken for the Rayleigh-type waves (RTW) possessing polarization in the sagittal plane for the coordinate system (see Fig. 1). In contrast to the LTW, the RTW can exist in both monocrystals and layered structures. However, surface waves with the anti-plane polarization (perpendicular to the sagittal plane) can also exist in piezoelectric monocrystals known as the surface Bleustein–Gulyaev type waves (BGTW).[2,3] Note that one of the BGTW discoverers states in Ref. 4 that such SAWs cannot exist in cubic piezoelectrics. Indeed, Bleustein[2] has noted that they cannot exist in (001) [100] propagation direction for the piezoelectrics. However, Gulyaev and Hickernell note that in 1966, Kaganov and Sklovskaya[6] studied the Love-wave-polarized SAWs in cubic piezoelectrics. Recent reviews of shear SAWs in solids can be found in Refs. 7, 8. The single-mode dispersive BGTW[9] propagate in layered systems, and they can be treated as the LTW first type (lowest-order mode), while an infinite number of LTW modes belong to the LTW second type. That is an analogy with the first (lowest-order mode) and second types of dispersive RTW. Note that all wave numbers k_3 for both the thin film and substrate should be imaginary/complex with $\chi_3 > 0$ for the dispersive BGTW and RTW first type. One can also read about the SAW types in the very famous and classical issues,[10–13] the book[10] of which describes SAW applications for signal processing. Note that today the LTWs are widely used in dispersive SAW filters and sensors, and of all known sensors, LTW SAW devices have the highest sensitivity.[14–17]

In addition to the well-known LTW and RTW SAW types with all $\chi_3^{(n)} > 0$ in $k_3^{(n)} = k_0^{(n)} - j\chi_3^{(n)}$ for a substrate, new types of slow SAWs possessing single mode with the anti-plane polarization and all $\chi_3^{(n)} < 0$ in $k_3^{(n)} = k_0^{(n)} + j\chi_3^{(n)}$ were discussed in Ref. 18 studying wave propagation in the layer-on-substrate structures. Indeed, such SAWs called the slow surface Zakharenko-type waves (SSZTWs) can propagate, for which substrate wave numbers along the x_3-axis are taken all with positive imaginary parts in Fig. 1 coordinate system. According to Ref. 18, the three-partial SSZTW3 with the Love wave polarization can exist with both the conditions $V_t^L > V_t^S$ and $V_t^L < V_t^S$ in contrast to the LTW3 existence single condition $V_t^L < V_t^S$. However, the SSZTW3 existence condition $V_t^L < V_t^S$ demands another additional condition on shear elastic constants $C_{44}^L > C_{44}^S$. As soon as both existence conditions are fulfilled, the SSZTW3 mode starts with zero-phase velocity at large values of kh (k is the wave number in direction of wave propagation, and h is the layer thickness) and approaches some maximum velocity $V_{tm} < V_t^L$ at $kh \to +\infty$. The SSZTW3 phase V_{ph} and group V_g velocities are studied in this paper. Note that the conditions $C_{44}^L > C_{44}^S$ and $V_t^L < V_t^S$ are also true for piezoelectrics that must be studied in future. It is thought that slow in-plane polarized SAWs can also exist.

Note that the SSZTW3 V_{ph} behavior, such as $V_{ph}(kh \sim 1 \text{ to } 3) = 0$ and $V_{ph}(kh \to +\infty) = V_{tm}$, is similar to the V_{ph} behavior of the asymmetric (*flexural*) A_0 mode of in-plane polarized Lamb-type waves in plates, for which there are $V_{ph}(kh = 0) = 0$ and $V_{ph}(kh \to +\infty) = V_R$ with the RTW velocity V_R. The analogy between the dispersive SSZTW and Lamb-type waves allows the use of the SSZTW3 single mode in technical devices instead of the Lamb wave A_0 mode. It is noted that different liquid and vapor sensors are manufactured using the Lamb wave A_0 mode. Therefore, it is possible to introduce some Lamb wave applications studied in Refs. 19–25. The most popular materials for studying the Lamb waves are Si and Al. Aluminum aircraft wings can be nondestructively inspected, and minimum dispersion[25] should occur. It is thought that the most suitable case for the SSZTW application is their usage in such microelectromechanical system (MEMS) structures as the capacitive micromachined ultrasonic transducers (CMUTs). Today, the Lamb wave CMUTs[19] in isotropic and nonpiezoelectric plates (membranes) are more preferable compared with piezoelectric plates. It is also thought that technological processes of CMUT manufacturing can be simplified working with the SSZTWs: the thin-film deposition single step for the SSZTW CMUT manufacturing process, but many steps in the Lamb wave CMUT manufacturing process, utilizing the sacrificial layer method.

The following section describes the theory for the SSZTW3 existence in the layered systems using nonpiezoelectric anisotropic materials. Section 3 shows the phase and group velocities' behavior. Section 4 further investigates the velocities with discussions about possible applications.

2. Slow Waves in Layered Systems

SAW two-layer structures, consisting of a layer on a substrate, can be treated as plates, one side of which represents vacuum–solid interface, and the opposite side is coupled with a solid substrate (see Fig. 1). The substrate usually localizes wave motion along the negative values of the x_3-axis at the layer–substrate interface. That can be achieved by material choice for both the layer and substrate. Thus, such structures represent waveguides, in which waves propagate along the x_1-axis within the layer. The constitutive equations for an anisotropic material can be expressed in terms of the strains τ related to mechanic displacements: $\tau_{ij} = (\partial U_i/\partial x_j + \partial U_j/\partial x_i)/2$. The governing mechanical equilibrium is written using stress σ as follows: $\partial\sigma_{ij}/\partial x_j = 0$. However, equations of motion must be separately written for each layer studying the layered structures. The equations of motion, omitting the piezoelectric/piezomagnetic effect as well as the elasto/electro-optic effect, can be written using the famous works[10–13,26] on waves in solids:

$$C_{ijkl}\frac{\partial^2 U_l}{\partial x_j \partial x_k} - \rho\frac{\partial^2 U_i}{\partial t^2} = 0\,, \tag{1}$$

where ρ is the mass density. The elasticity tensor components $C_{ijkl} = (1/V)[\partial^2 E/(\partial\Theta_{ij}\partial\Theta_{kl})]$ with the Eulerian strain tensor components Θ_{ij} and Θ_{kl} are thermodynamically determined using the enthalpy $H = E + PV$ with E, P, and V denoting the internal energy, pressure, and volume, respectively. Physical properties of crystals and their representation by tensors and matrices can be read in detail in the classic book[27] by Nye. Solutions for the displacement components U_i in Eq. (1) can be readily found using the plane wave approximation:

$$U_i = U_{i0}\exp[j(k_1x_1 + k_3x_3 - \omega t)]\,, \tag{2}$$

where U_{i0} is an initial amplitude, $\omega = 2\pi v$ and t are the angular frequency and time, respectively. The wavevector $\mathbf{K}_s$ components k_1 and k_3 are the projections onto the x_1 and x_3-axes in Fig. 1; $j = (-1)^{1/2}$. Substituting the U_i from (2) into (1), one can obtain equations of motion in the following tensor view:

$$(GL_{ij} - \delta_{ij}\rho\omega^2)U_i = 0\,, \tag{3}$$

where $GL_{ij} = C_{ijkl}k_lk_k$ are the GL-tensor components in the Green–Christoffel equation. δ_{ij} is the Kronecker delta: $\delta_{ij}(i = j) = 1$ and $\delta_{ij}(i \neq j) = 0$.

The theoretical description[10,12,13] of wave propagation in solids in the common case states that there are such propagation directions for both piezoelectrics and nonpiezoelectrics, in which the "pure" waves can exist. They can have the anti-plane polarization perpendicular to the sagittal plane possessing single mechanical displacement component U_2 independent from the other components U_1 and U_3. Also, "pure" waves can have the in-plane polarization in the sagittal plane when the U_1 and U_3 are coupled. Note that the "pure" waves can propagate in each propagation direction of isotropic materials. To realize the "pure" waves in nonpiezoelectric crystals, a chosen propagation direction should give the following zero components of the symmetric GL-tensor: $\mathrm{GL}_{12} = \mathrm{GL}_{21} = \mathrm{GL}_{23} = \mathrm{GL}_{32} = 0$. Dieulesaint and Royer also discuss possible cuts and directions for "pure" wave existence in crystals of 32 point groups of symmetry. For instance, the "pure" wave existence in cubic nonpiezoelectrics occurs in (001) [100] and (001) [110] directions. Therefore, the following corresponding equation can be readily separated from Eq. (3) to treat anti-plane polarized "pure" waves:

$$(GL_{22} - \rho\omega^2)U_2 = 0\,, \tag{4}$$

where GL_{22} is the GL-tensor nonzero component. U_2 is the displacement component along the x_2-axis. Equation (4) is true for almost all crystal symmetries from monoclinic to cubic, see Refs. 10, 12, 13.

For a thin film in the waveguide shown in Fig. 1, Eq. (4) expanding the GL_{22}-tensor component is written as follows:

$$GL^L_{22} - \rho^L\omega^2 = k^2C^L_{66} + 2kk^L_3C^L_{46} + (k^L_3)^2C^L_{44} - \rho^L\omega^2 = 0\,, \tag{5}$$

where the superscript L is used for the layer. C^L_{66}, C^L_{46}, C^L_{44}, and ρ^L are the layer material constants assuming bulk elastic properties for the layer, and k^L_3 is the wavevector projection onto the x_3-axis. After some transformations in Eq. (5), two polynomial roots can be found as follows:

$$k_3^{L(1.2)} = -\frac{C^L_{46}}{C^L_{44}}k \pm j\zeta_3 \quad \text{with} \quad \zeta_3 = \alpha^L_f k\left[1 - \left(\frac{V_{ph}}{\beta^L}\right)^2\right]^{1/2} \quad (V_{ph} < \beta^L)\,, \tag{6}$$

where $V_{ph} = \omega/k$ is the phase velocity, $\alpha^L_f = [C^L_{66}C^L_{44} - (C^L_{46})^2]^{1/2}/C^L_{44}$ is the elastic anisotropy factor. The velocity equivalent β^L is defined as $\beta^L = V^L_{t4}\alpha^L_f$ with $V^L_{t4} = (C^L_{44}/\rho^L)^{1/2}$. In some highly symmetric propagation directions, for example, in [100] direction for nonpiezoelectric cubic crystals, there is $C_{66} = C_{44}$ resulting in $V_{t4} = V_{t6}$, where $V_{t6} = (C_{66}/\rho)^{1/2}$ represents the speed of the bulk shear-horizontal wave. According to Ref. 12, there is $\beta < V_t$ with the energy conservation condition $C_{66}C_{44} > C^2_{46}$ for anisotropic case. It is noted that in this case there are complex values of $k_3^{L(1,2)}$ for $V_{ph} < \beta^L$, while two real roots should be in Eq. (6) for LTWs with the $V_{ph} > \beta^L$ in the layered system shown in Fig. 1. Note that both positive and negative values of the layer damping wave number ζ_3 are taken in calculations.

Expanding the corresponding GL_{22}-tensor component for the substrate in Eq. (3) and using the superscript S, the following equation must be solved in order to find values of k^S_3:

$$GL^S_{22} - \rho^S\omega^2 = k^2C^S_{66} + 2kk^S_3C^S_{46} + (k^S_3)^2C^S_{44} - \rho^S\omega^2 = 0\,, \tag{7}$$

two complex roots of which are written as follows:

$$k_3^{S(1,2)} = -\frac{C^S_{46}}{C^S_{44}}k \pm j\chi_3 \quad \text{with} \quad \chi_3 = \alpha^S_f k\left[1 - \left(\frac{V_{ph}}{\beta^S}\right)^2\right]^{1/2} \quad (V_{ph} < \beta^S)\,. \tag{8}$$

Analogically, the elastic anisotropy factor for the substrate is $\alpha^S_f = [C^S_{66}C^S_{44} - (C^S_{46})^2]^{1/2}/C^S_{44}$, and the velocity equivalent β^S is equal to $\beta^S = V^S_{t4}\alpha^S_f$ with $V^S_{t4} =$

$(C_{44}^S/\rho^S)^{1/2}$. In Eqs. (5)–(8), the wave number $k = k_1 = k_1^L = k_1^S$ is the wavevector $\mathbf{k}$ component along the x_1-axis, $k = 2\pi/\lambda$ with λ being the wavelength. It is noted that for the free space, it is taken $\mathrm{GL}_{ij} = 0$ due to all $C_{ijkl} = 0$. It is clearly seen in Eq. (8) that the substrate damping wave number χ_3 can be both positive and negative due to the square root dependence. For LTWs, the dispersion relations, showing dependence of the damping wave number χ_3 for a substrate on the real wave number k_3 for a layer, give positive values of $\chi_3 : \chi_3(k_3 > 0) > 0$. Therefore, the sign of χ_3 is taken to be negative in Eq. (8) in order to have surface waves. However, for SSZTWs, the dispersion relations $\chi_3(\zeta_3)$ give negative values of $\chi_3\{\chi_3(\zeta_3 > 0) < 0\}$ depending on imaginary layer wave number ζ_3. Therefore, the χ_3 sign should be positive giving SAWs. That is also true for piezoelectrics, where all substrate wave numbers $\chi_3^{(n)}$ with positive imaginary parts should be chosen for finding the SSZTWs in the Fig. 1 coordinate system instead of the substrate wave numbers $\chi_3^{(n)}$ with negative imaginary parts for finding LTWs.

It is necessary to account for mechanical boundary conditions on both sides of the thin film in Fig. 1. First of all, it is required that there is continuity of the displacement component U_2 at the interface $x_3 = 0$ between the layer and substrate, as well as continuity of the stress tensor normal component $\mathrm{ST}_{32} = C_{44}k_3 + C_{46}k_1$. At the free surface $x_3 = h$, where h is the layer thickness, the displacement component U_2 is arbitrary. Therefore, the single requirement represents equality to zero of the stress tensor component, $\mathrm{ST}_{32} = 0$. The boundary conditions result in the following set of homogeneous equations:

$$\begin{pmatrix} 1 & -1 & -1 \\ C_{44}^S k_3^S + C_{46}^S k & -C_{44}^L k_3^{L(1)} + C_{46}^L k & -C_{44}^L k_3^{L(2)} + C_{46}^L k \\ 0 & [C_{44}^L k_3^{L(1)} + C_{46}^L k]\exp(jk_3^{L(1)}h) & [C_{44}^L k_3^{L(2)} + C_{46}^L k]\exp(jk_3^{L(2)}h) \end{pmatrix} \times \begin{pmatrix} f^S U_2^S \\ f^{L(1)} U_2^{L(1)} \\ f^{L(2)} U_2^{L(2)} \end{pmatrix} = 0\,. \tag{9}$$

There are the so-called weight coefficients $f^{L(1)}$, $f^{L(2)}$, and f^S in Eq. (9), as well as the displacement partial components $U_2^{L(1)}$, $U_2^{L(2)}$, and U_2^S. Expanding the third-order boundary conditions' determinant (BCD3) of matrix in Eq. (9), the following dispersion relation appears, using Eqs. (6) and (8):

$$\chi_3 h(\zeta_3 h > 0) = -a\zeta_3 h \tanh(\zeta_3 h) < 0 \quad \text{with} \quad a = C_{44}^L/C_{44}^S\,. \tag{10}$$

It is clearly seen in Eq. (10) that positive and negative values of the layer wave number $\zeta_3 h$ are equivalent. Therefore, only positive values of $\zeta_3 h$ can be taken for the treatment.

The phase velocity V_{ph} represents the well-known function of the angular frequency ω and wave number k and is defined as follows:

$$V_{ph} = \frac{\omega(\zeta_3)}{k(\zeta_3)}\,. \tag{11}$$

The functions $\omega(\zeta_3)$ and $k(\zeta_3)$ are found from definition of the wave numbers $\zeta_3 h$ and $\chi_3 h$ in Eqs. (6) and (8), respectively. After some transformations, they are written as follows:

$$\omega(\zeta_3) = \frac{V_{t4}^L}{b}\frac{\alpha_f^L}{\alpha_f^S}\left[-\zeta_3^2\left(\frac{\alpha_f^S}{\alpha_f^L}\right)^2 + \chi_3^2\right]^{1/2}, \tag{12}$$

$$k(\zeta_3) = \frac{1}{b\alpha_f^S}\left[-\zeta_3^2\left(\frac{V_{t4}^L}{V_{t4}^S}\right)^2 + \chi_3^2\right]^{1/2}, \tag{13}$$

where there is the constant $b = [1 - (\beta^L/\beta^S)^2]^{1/2}$, which depends on both the velocity equivalents for the layer β^L and substrate β^S. It is possible to multiply by the layer thickness h both the left-hand and right-hand sides of Eqs. (12) and (13) in order to deal with nondimensional values of $\zeta_3 h$ and function $\chi_3 h(\zeta_3 h)$ defined from boundary conditions in Eq. (10). It is clearly seen in Eqs. (12) and (13) that there is no dependence on the sign of the function $\chi_3 h(\zeta_3 h)$, which can be both positive and negative. However, the substrate wave number χ_3 sign for finding slow SAWs should be chosen to be opposite to the one for finding LTWs that was discussed above.

This paper studies slow SAW propagation in the layered systems with the condition for the velocity equivalent, such as $\beta^L < \beta^S$. According to Ref. 18, values under square roots in Eqs. (12) and (13) should be positive real, in order to have positive real functions $\omega(\zeta_3)$ and $k(\zeta_3)$. That gives two inequalities for analyzing

$$0 \le D^2\tanh^2(\zeta_3 h) - 1 \quad \text{and} \quad 0 \le D^2\tanh^2(\zeta_3 h) - \left(\frac{\beta^L}{\beta^S}\right)^2 \quad \text{with} \quad D = a\frac{\alpha_f^L}{\alpha_f^S}\,. \tag{14}$$

It is clearly seen in Eq. (14) that $D\tanh(\zeta_3 h) \ge 1$ and $D\tanh(\zeta_3 h) \ge \beta^L/\beta^S$. Because $\beta^L < \beta^S$, it is necessary and sufficient to treat only the first inequality. It is well-known that the hyperbolic tangent is confined between zero and unity for $\zeta_3 h \ge 0$. Finally, the following requirements for solutions existence can be written for such slow dispersive waves:

$$\beta^S > \beta^L \quad \text{and} \quad D \ge 1\,. \tag{15}$$

In this case, the V_{ph} starts with its minimum value of $V_{ph} = 0$ for $\zeta_3 h > 0$. It is noted that for $D = 1+\delta$ with $\delta \to 0$, the V_{ph} will start with $V_{ph} = 0$ at a large value of $\zeta_3 h$. Such dispersive solutions exist in the following $\zeta_3 h$, kh, and V_{ph} ranges:

$$\zeta_0 h \le \zeta_3 h \le +\infty \quad \text{with} \quad \zeta_0 h = \mathrm{Arctanh}(1/D)\,, \tag{16}$$

$$k_0h \le kh(\zeta_3 h) \le +\infty \quad \text{with} \quad k_0h = \frac{1}{b\alpha_f^S}\text{Arctanh}(1/D)\left[-\left(\frac{V_{t4}^L}{V_{t4}^S}\right)^2 + \left(\frac{a}{D}\right)^2\right]^{1/2}, \tag{17}$$

$$0 \le V_{ph} \le V_{tm} \quad \text{with} \quad V_{tm} = \beta^L\left[\frac{D^2-1}{D^2-(\beta^L/\beta^S)^2}\right]^{1/2} \quad \text{and} \quad D^2 > 1\,. \tag{18}$$

It is clearly seen in Eq. (18) that the velocity $V_{tm} < \beta^L$ because $\beta^L < \beta^S$. This type of three-partial slow surface Zakharenko waves (SSZTW3) in Eqs. (16)–(18) has the single dispersive mode starting at $k_0h > 0$ according to Eq. (17), but not at $k_0h = 0$. Also, it was numerically found that $k_0h = \zeta_0 h$ for $V_{ph} = 0$. The mode starting with $k_0h > 0$ occurs due to existence of energy-dissipative waves with the imaginary frequency $j\omega$ in the kh-range $0 < kh < k_{01}h$ that was shown and discussed in Ref. 18. It is noted that such dissipative waves can even give real phase and group velocities, $V_{ph1} = j\omega/jk$ and $V_{g1} = jd\omega/jdk$. Also, Zakharenko[18] discusses the second type of SSZTW3 propagating in layered structures consisting of a rigid layer on a substrate, $\beta^L > \beta^S$, and possessing a single dispersive mode, which exists in the kh-range: $0 < kh < k_{02}h$ without energy dissipation for real frequency ω. Peculiarities of the SSZTW3 second type can be studied in future. Indeed, real phase and group velocities, $V_{ph2} = j\omega/jk$ and $V_{g2} = jd\omega/jdk$, can also be found here for $kh > k_{02}h$.

Figure 2 shows the functions $\omega h(\zeta_3 h)$ and $kh(\zeta_3 h)$ for the SSZTW3 first type using Eqs. (12) and (13) for some layered systems listed in Table 1. It is clearly seen that they depend on the function $\chi_3 h(\zeta_3 h)$ determined by the dispersion relation in Eq. (10). Therefore, it is necessary to mathematically analyze the behavior of the function $\chi_3 h(\zeta_3 h)$ calculating the following first derivative:

$$\frac{d\chi_3 h}{d\zeta_3 h} = -a\left[\tanh(\zeta_3 h) + \frac{\zeta_3 h}{\cosh^2(\zeta_3 h)}\right]. \tag{19}$$

It is clearly seen in Eq. (19) that the first derivative goes to $-a$ for $\zeta_3 h \to \infty$ since hyperbolic tangent approaches unity. The behavior of the function $\chi_3 h(\zeta_3 h)$ is

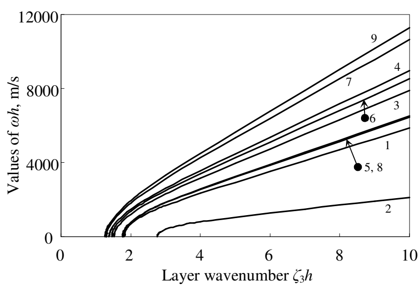

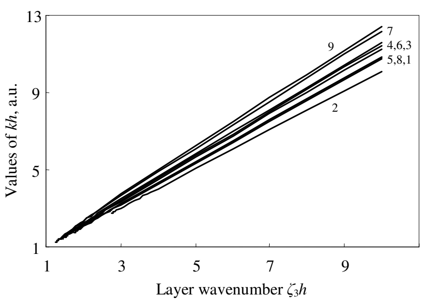

Fig. 2. The dependences (a) $\omega h(\zeta_3 h)$ and (b) $kh(\zeta_3 h)$ using their functions in Eqs. (12) and (13). Crystal names for numbers (1)–(9) are given in Table 2.

Table 1. The acoustic crystal characteristics taken from Refs. 28, 29.

Crystal name	Density (kg/m^3)	C_{44} ($\times 10^{10}$ N/m^2)	C_{66} ($\times 10^{10}$ N/m^2)	C_{46} ($\times 10^{10}$ N/m^2)	V_{t6}(m/s)	V_{t4}(m/s)	α_f	β(m/s)	D^2	V_{tm} (m/s)
Au	19754	4.60	4.60	—	1525.989	1525.989	1	1525.989	—	—
Muscovite	2820	1.65	7.20	−0.32	5052.912	2418.897	2.0799	5031.088	1.7966	1043.193
Albite	2630	1.73	3.20	−0.25	3488.166	2564.751	1.3523	3468.420	3.8659	1348.066
Anorthite	2760	2.35	4.15	−0.12	3877.658	2917.960	1.3279	3874.794	2.1729	1163.438
Hyalophane	2646	1.36	3.54	−0.17	3657.688	2267.120	1.6085	3646.694	4.4217	1369.784
Zincite(ZnO)	5642	4.245	4.429	—	2801.763	2742.946	1.0214	2801.763	1.1255	593.828
Hydroapatite	3218	3.96	4.75	—	3841.968	3507.960	1.0952	3841.968	1.1249	548.452
Ftorapatite	3218	4.43	4.70	—	3821.694	3710.298	1.0300	3821.694	1.0163	210.353
TeO_2	5990	2.65	6.59	—	3316.876	2103.340	1.5770	3316.876	1.2117	702.069
NaO	2805	4.05	4.05	—	3799.803	3799.803	1	3799.803	1.2900	773.541
$RbMnF_3$	4317	3.19	3.19	—	2718.343	2718.343	1	2718.343	2.0794	1193.601
CaF_2	3180	3.37	3.37	—	3255.378	3255.378	1	3255.378	1.8632	1105.923
SrF_2	4240	3.20	3.20	—	2747.211	2747.211	1	2747.211	2.0664	1188.558
Fe_2TiO_4	4836	3.96	3.96	—	2861.570	2861.570	1	2861.570	1.3494	874.004
ZnSe	5264	3.92	3.92	—	2728.884	2728.884	1	2728.884	1.3770	908.243
InSb	5790	3.04	3.04	—	2291.382	2291.382	1	2291.382	2.2896	1275.426
ZnTe	5636	3.12	3.12	—	2352.837	2352.837	1	2352.837	2.1737	1248.633
$Bi_4(GeO_4)_3$	7120	4.36	4.36	—	2474.590	2474.590	1	2474.590	1.1131	599.539
$CaMoO_4$	4340	3.69	4.61	—	3259.159	2915.871	1.1177	3259.159	1.2439	744.509
$CaWO_4$	6010	3.35	3.87	—	2537.571	2360.941	1.0748	2537.571	1.6321	1076.393

Here there are the velocity equivalent $\beta = \alpha_f V_{t4}$ and the speed $V_{t6} = (C_{66}/\rho)^{1/2}$ of the bulk shear wave. The last two columns give features for Au/crystal structures: $D^2 = (a\alpha_f^L/\alpha_f^S)^2$ and V_{tm} from Eq. (18).

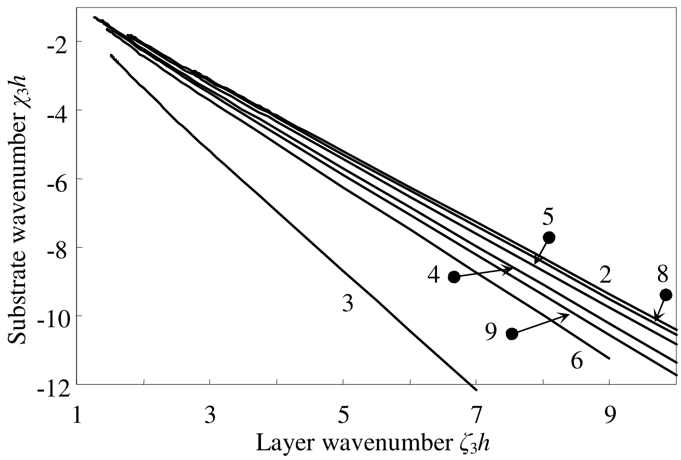

Fig. 3. The dependences $\chi_3 h(\zeta_3 h)$ for crystals with corresponding numbers (1)–(9) given in Table 2.

shown in Fig. 3 for layered systems, consisting of the Au-layer on different substrates listed in Table 1. Gold has high material density that results in slow velocity V_{t6} compared with the other crystals listed in the table, which shows some substrate materials with suitable shear elastic constants being slightly larger than that for gold, $C_{44}^S > C_{44}^L$, in order to have the velocity V_{tm} as small as possible. In the table, the materials are listed, which give the velocity $V_{tm} \sim 1000$ m/s and below. It is noted that the smallest velocity V_{tm} in the table is for the layered structure consisting of the Au-layer on the substrate of ftorapatite ($Ca_{10}(PO_4)_6F_2$): $V_{tm} \sim 210$ m/s. The higher derivatives of the function $\zeta_3 h(\zeta_3 h)$ are given by the appendix formulae (A1) and (A2), and they are used for further investigations of the phase and group velocities.

The displacements behavior of the SSZTW3 first type studied in this paper can be found in both the layer and substrate as follows:

$$\begin{aligned} U_2 &= U_0 \frac{\cosh[\zeta_3(x_3 - h)]}{\cosh(\zeta_3 h)} \exp[j(k_1 x_1 - \omega t] \quad (0 \le x_3 \le +h)\,, \\ U_2 &= U_0 \exp(-\chi_3 \chi_3) \exp[j(k_1 x_1 - \omega t)] \quad (x_3 \le 0, \chi_3 < 0)\,. \end{aligned} \tag{20}$$

In Eq. (20), the negative values of substrate wave number χ_3 are calculated with the dependence $\chi_3 h(\zeta_3 h)$ from Eq. (10). Figure 4 shows the SAW displacement behavior for the layered structures: Au/ftorapatite and Au/TeO_2. Paratellurite (TeO_2), also called tellurium dioxide, belongs to the tetragonal crystal class 422 and is distinguished by extremely high elastic anisotropy. Paratellurite is a piezoelectrics and is one of the crystals mostly used in acousto-optics. Hence, the SSZTW3 first type in the Au/TeO_2 system can be studied in future to notify the piezoelectricity influence.

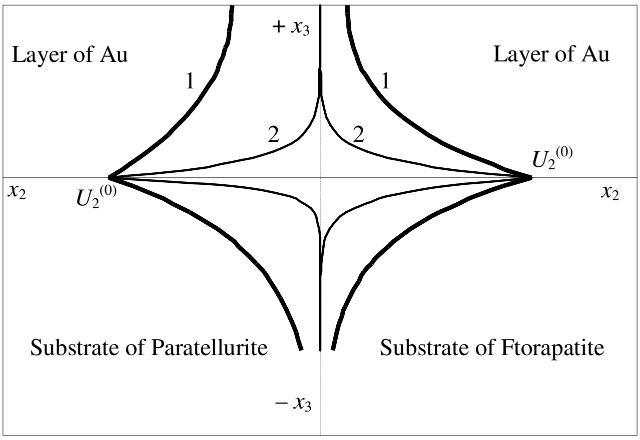

Fig. 4. The displacement behavior for the layered structures such as Au/ftorapatite and Au/paratellurite, using different values of $\chi_3 h$ and $\zeta_3 h$: (1) $\chi_3 h(\zeta_3 h \sim 1.519) \sim -2.395$ for Au/paratellurite and $\chi_3 h(\zeta_3 h \sim 2.756) \sim -2.839$ for Au/ftorapatite; and (2) $\chi_3 h(\zeta_3 h = 10) = -17.3585$ for Au/paratellurite and $\chi_3 h(\zeta_3 h = 10) = -10.384$ for Au/ftorapatite.

For nonsurface waves, sample displacement behavior was shown in Ref. 18. It is clearly seen in Fig. 4, using values of the velocity V_{tm} from Table 1, that there is a smaller damping in the layer from the interface toward the layer free surface in layered structures with higher velocity V_{tm}, because the single mode starts at a smaller value of kh. Therefore, in suitable layered systems with a high velocity V_{tm} there will be a weak damping in the layer at $kh \to k_0 h$ from the interface toward the layer free surface. For large values of kh, when the V_{ph} approaches the velocity V_{tm}, the displacements are localized at the interface and can be readily found there. It is noted that such slow SAWs can exist due to the free surface influence, and interfacial waves (like Stoneley-type waves with the in-plane polarization) with the anti-plane polarization propagating along the interface of two solids do not exist at small values of kh. It is noted that when nondispersive interfacial Stoneley-like waves propagate along the interface between two solid half-spaces, they are localized at the interface and can exist in both configurations: a rigid half-space (layer) on a soft substrate (half-space) and the soft half-space on the rigid substrate, showing the same propagating velocity for both configurations. That completely differs from the SSZTW existence, which starts at $V_{ph}(k_{01}h) = 0$ approaching the velocity V_{tm} at $kh \to \infty$ for the configuration of the soft layer on the rigid substrate. However, for the configuration of the rigid layer on the softer substrate, the SSZTW-V_{ph} starts at $kh = 0$ with the bulk wave velocity V_t^S for the substrate, but not with the velocity V_{tm}, and reduces to zero at $k_{02}h$, according to Ref. 18. Hence, it is possible to state that there is no analogy between the SSZTWs with the velocity V_{tm}, existing due to the influence of the layer free surface, and completely interfacial Stoneley-like waves.

3. Phase and Group Velocities and Their First Derivatives

It is thought that both the V_{ph} and the derivative of V_{ph} are the most important wave characteristics. The V_{ph} for different structures shown in Fig. 5(a) was calculated with formulae (11)–(13) for the structures listed in Table 2. That is probably the most convenient case to calculate it. Also, the V_{ph} can be calculated from Eq. (10) using the definitions in Eqs. (6) and (8). The V_g is defined as follows:

$$V_g = \frac{d\omega}{dk}\,. \tag{21}$$

The V_g can be readily evaluated with the following numerical approximation, using the appendix formulae (A3) and (A4):

$$V_g = \frac{d\omega h}{d\zeta_3 h}\bigg/\frac{dkh}{d\zeta_3 h}\,. \tag{22}$$

Using Eqs. (A3) and (A4), the V_g in (23) depends on $(1/V_{ph})$ and becomes infinity for zero V_{ph}. However, it is thought that there should be $V_g = V_{ph} = 0$ manifesting mode beginning for dispersive waves. Therefore, the V_g can be calculated with known V_{ph} using the other formula. Indeed, there is the following dependence[30] of

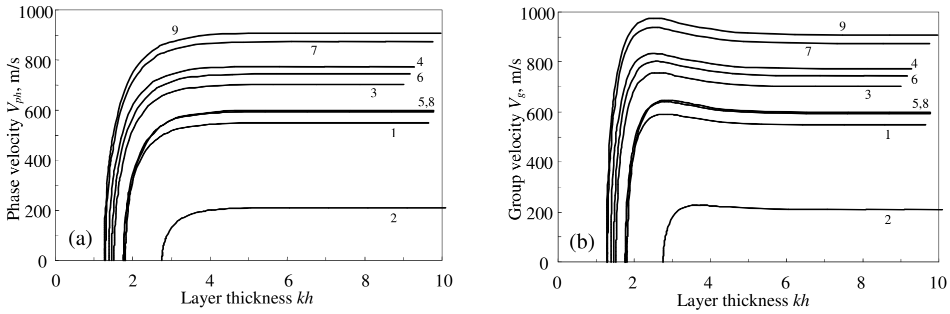

Fig. 5. The phase (a) and group (b) velocities. Crystal names for numbers (1)–(9) are given in Table 2.

Table 2. The effective masses for the SSZTW3 first type at the wave number $k \to k_0$, which were calculated with formula (27) taking the layer thickness $h = 1$ μm for the Au/crystal systems listed in Table 1.

Crystal	(1) Hydroapatite	(2) Ftorapatite	(3) Paratellurite (TeO_2)
Mass $\mu^*(\times 10^{-38}$ kg)	~ 2.7	~ 3.2	~ 2.2
Crystal	(4) NaO	(5) Zincite (ZnO)	(6) Powellite ($CaMoO_4$)
Mass $\mu^*(\times 10^{-38}$ kg)	~ 1.3	~ 2.4	~ 1.5
Crystal	(7) Fe_2TiO_4	(8) $Bi_4(GeO_4)_3$	(9) ZnSe
Mass $\mu^*(\times 10^{-38}$ kg)	~ 1.6	~ 1.8	~ 1.2

For comparison, the mass of a free electron is 0.911×10^{-30} kg.

the V_g on the V_{ph}, kh, and derivative of V_{ph} with respect to kh:

$$V_g = V_{ph} + (k - k_0)h\frac{dV_{ph}}{dkh}\,. \tag{23}$$

It is noted that it is possible to use in Eq. (23) values of $(k - k_0)$ instead of values of k for the case of $V_g(k_0h) = V_g(k_0h) = 0$ in order to receive true V_g behavior, because the mode beginning starts at $k_0h \neq 0$. However, usage of $(k - k_0)$ instead of k in $dV_{ph}/dkh = dV_{ph}/d(kh - k_0h)$ and other derivatives written below must give the same result, because k_0h is constant. Also, it is clearly seen in Eq. (23) that for very small values of $(k-k_0)h$ resulting in $dkh = (k-k_0)h$, the relationship $V_g = 2V_{ph}$ must be fulfilled for a free quasi-particle (QP) propagating in vacuum. The dependence $V_g(kh)$ calculated with formula in Eq. (23), using the appendix formula (A5), is shown in Fig. 5(b) for the structures listed in Table 2. Both V_g and V_{ph} approach the corresponding maximum velocity V_{tm} at $kh \to \infty$, which should be lower than the corresponding speeds V_t for each studied layered structure.

Equation (23) states that as soon as some dependence V_{ph}(kh) appears, the V_g is unequal to the V_{ph}, except mode beginning at $kh = 0$ or $kh = k_0h$. Therefore, the inequality between V_g and V_{ph} can be a dispersion indicator. It is possible to evaluate the value of $\max(V_g - V_{ph})$ treating the case of $V_g > V_{ph}$. From Eq. (23) it is possible to write the following equality:

$$\max(V_g - V_{ph}) = \max\left[kh\frac{dV_{ph}}{dkh}\right]. \tag{24}$$

The extreme point becomes equal to zero by applying the well-known convenient mathematical procedure giving the following equation for analysis:

$$\frac{d(V_g - V_{ph})}{dkh} = \frac{dV_{ph}}{dkh} + kh\frac{d^2V_{ph}}{d(kh)^2} = 0\,, \tag{25}$$

from which a kh-domain for maximum difference between V_g and V_{ph} can be readily evaluated.

Figure 6 shows the V_{ph} together with the V_g for the sample layered structure: Au/ftorapatite possessing the smallest velocity V_{tm}. The figure insertion shows deviation of the V_{ph} and V_g from the linear dependencies $V_{ph}(k)$ and $V_g(k)$ with the QP relationship $V_g = 2V_{ph}$ at small values of $(k - k_0)$. The V_g looks like a hybridization of the velocities V_{g1} and V_{g2} starting with the velocity V_{g1} at $kh \to k_0h$ and possessing one maximum in the kh-range: $k_0h < kh < \infty$. Both the velocities V_g and V_{g2} approach the velocity V_{tm} at $kh \to \infty$. The kinetic energy E_k at small $(k - k_0)$ can be given by the well-known Quantum Physics formula describing the energy dependence on the angular frequency ω as well as on the wave number k. Namely, the energy of a free QP in vacuum $E_k = \hbar\omega = p^2/2M$ or $E_k = \hbar(\omega - \omega_0) = (p - p_0)^2/2M$ represents common dispersion relation of a quantum system, where M represents a QP mass m or an effective mass μ^*. $\hbar = 1.05459 \times 10^{-34}$Js is the quantum Planck's constant having the physical sense of action quantum and dimension of impulse momentum. The particle quasi-impulse

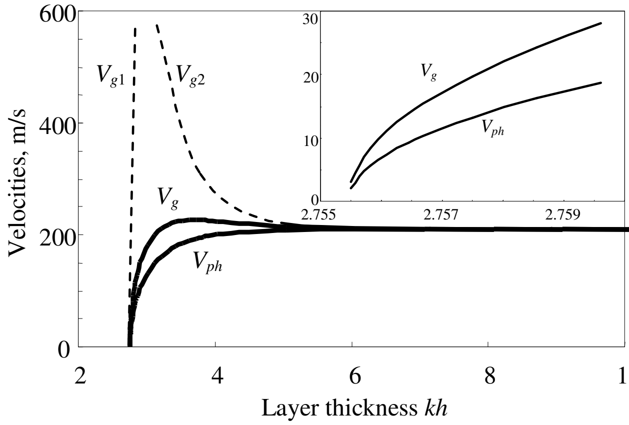

Fig. 6. The phase and group velocities for the Au/ftorapatite structure. The group velocities V_{g1} and V_{g2} represent the free quasi-particle approximation at small values of $(k - k_0)h$ and approximation of Eq. (22) for $kh \to \infty$, respectively. The insertion shows the functions $V_g(kh)$ and $V_{ph}(kh)$ with the relationships $V_g \sim 2\ V_{ph}$ for small values of $(k - k_0)h$.

$p = \hbar k = MV_g(p_0 = \hbar k_0)$ linearly depends on the wave number k. Excluding the energy dependence on mass, the kinetic energy can be represented by the following formula: $E_k = \hbar k V_g/2 = \hbar k V_{ph}$. It is necessary here to state that mass possessing is the consequence of wave properties, namely the straight line dependencies $V_g(k)$ and $V_{ph}(k)$ in the dispersion relations giving the following definition: $M = \hbar k/V_g = \hbar k dk/d\omega$. This definition states that mass is a result of continuous changes in time and space and represents the wave motion consequence in the problem of wavelet-corpuscular dualism. Table 2 gives the masses calculated with the following formula, using $V_g(k_0) = 0$:

$$\mu^*(k \to k_0) = \frac{\hbar(k - k_0)}{V_g(k)} = \frac{\hbar(k - k_0)}{2V_{ph}(k)}\,, \tag{26}$$

which gives mass of a soliton-like phonon. It is noted that dispersive waves possessing the dispersion relationship $V_g = 2V_{ph}$ of a free QP can be called solitons. In Table 2, effective masses can be compared with the mass of a free electron: $m_{e-} = 0.911 \times 10^{-30}$ kg. The effective masses are smaller than m_{e-} giving a unique feature for such very light QPs. Using values of V_{tm} listed in Table 1, note that there is dependence between the velocity V_{tm} and effective mass: the mass is larger in such layered structure in which the velocity V_{tm} is smaller. Such effective mass dependence on the layer thickness h as a larger mass corresponds to a smaller h and *vice versa*, could be due to occurrence of a greater mass compensation for a larger h because the layer boundaries are moved further from each other. It is thought that the values of the effective mass listed in Table 2 can further reduce down to $\sim 10^{-40}$ kg at $V_{ph} \to 0$, because the V_{ph} depends on kh quasi-linear (see the insertion in Fig. 6) but not linear that can be used for some applications concerning study of very light QPs.

It is obvious in Fig. 5(a) that the dispersive SSZTW3 single modes cannot possess the nondispersive Zakharenko-type waves (ZTW) at $k > k_0$ and $k < \infty$. The wave phenomenon called the nondispersive ZTW can exist in many structures,[30] where dispersive waves can propagate, and can be mathematically defined by the following formulas, using $(k - k_0)$ instead of k and $\omega_0 = \text{const}$ (it is possible to take $\omega_0 = 0$ for simplicity meaning zero potential energy, $E_p = \hbar\omega_0$) for the case:

$$dV_{ph}/d(k - k_0) = V_g(dV_{ph}/d\omega) = 0\,, \tag{27}$$

$$dV_{ph}/d(k - k_0) = (V_g - V_{ph})/(k - k_0)\,, \tag{28}$$

$$dV_{ph}/d\omega = V_{ph}(1 - V_{ph}/V_g)/\omega\,. \tag{29}$$

Note that ω_0 position on the energy scale must be determined from experiments. The first relationship between the derivatives of the V_{ph} in Eq. (27) shows that there is independence of the V_{ph} on both the frequency ω and wave number k. Note that dispersive waves are defined as dependence of the V_{ph} on both the ω and k. Equations (28) and (29) clarify that the equalities in Eq. (27) occur when the V_{ph} and V_g are equal in dispersion relations for the wave number $k \neq 0 (k > 0)$ and $k < \infty$. It is noted that the V_g cannot be equal to zero, except the situation when there is the following straight line behavior of the velocities: $V_g(k) = 2V_{ph}(k)$ at $k \to 0$ or $(k - k_0) \to 0$. That corresponds to a free QP existing in vacuum (or even forming "quasi-vacuum" that is possible to suggest), where k_0 is a nonzero wave number for zero kinetic energy $E_k = \hbar^2(k - k_0)^2/2\mu^*$ that frequently occurs in quantum systems.

The first derivatives of both the V_{ph} and V_g of the SSZTW3 first type are shown in Figs. 7(a) and 7(b), respectively. The formula for the dV_g/dkh is given by the following relationship, using Eq. (23):

$$\frac{dV_g}{dkh} = 2\frac{dV_{ph}}{dkh} + (k - k_0)h\frac{d^2V_{ph}}{d(kh)^2}\,, \tag{30}$$

where the derivatives of the V_{ph} are taken from the appendix formulae (A5) and (A6), respectively.

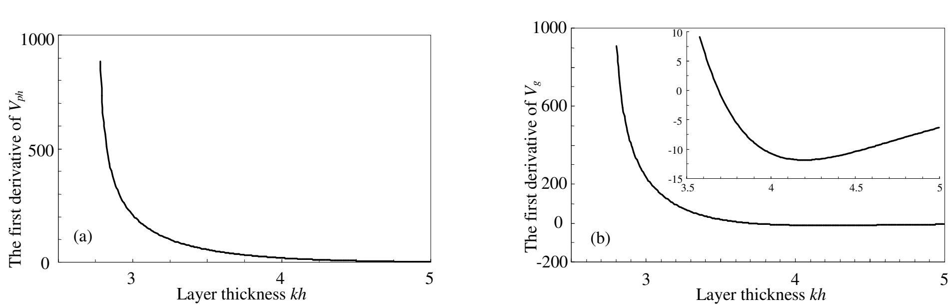

Fig. 7. The first derivatives of the phase (a) and group (b) velocities for the Au/ftorapatite structure. The insertion shows sign changing of the dV_g/dkh.

In addition to this study of the SSZTW3 second type existing in the case of a rigid layer on a soft half-space, there are also works concerning SAW existence in the same case. Kaibichev and Shavrov[31] have reported about new SAW existence with the $V_{ph} > V_{t1} > V_{t2}$, where V_{t1} and V_{t2} are the speeds of the corresponding shear transverse waves for the layer and half-space. They have treated the same dispersion equation $y = a_0 x \,\mathrm{Tan}(x)$, which is used for finding the LTW3-V_{ph}. However, they have noted that Dieulesaint and Royer in their famous book[10] have stated only single possibility for SAW existence representing LTW3 solutions of the equation $y = a_0 x \,\mathrm{Tan}(x)$ that is true. The other more complicated case of SAWs was studied in the work[32] by Gulyaev and Plessky. Such acoustic waves with the Love wave polarization are inhomogeneous, and they caused by a periodic structure on the monocrystal surface giving acoustic waves, which are slowing down. Also, slow flexural SAWs with the Rayleigh wave polarization in layered structures for the case of $\rho^L > \rho^S$ and $\mu^L > \mu^S$ (ρ and μ are the mass density and shear module) were studied by Viktorov *et al.*[33] using both theoretical and experimental approximations. The work[33] particularly gives an approximated formula for V_{ph} calculations, which corrects a previous formula taken from Ref. 34 and is coupled with the V_{ph} of zero-order mode of asymmetric Lamb-type waves (flexural plate waves). As the result of their approximations, a maximum error for V_{ph} calculation was up to 30%, and the same for V_g calculation was even over 50%. Note that several experimental points of measured V_g of their slow SAW with the 50% errors do not clarify the problem: which V_g was actually measured, the slow SAW or the bulk shear wave? Such a big interest in finding slow SAW caused by their unique properties: very small V_{ph} can be reached by proper choice of kh that can be quite useful in a set of technical applications.

4. Higher Derivatives and Their Possible Applications

It is necessary to study the SSZTW3 first type more widely due to their possible applications in different MEMS technical devices. Note that such type of slow SAWs can exist in the same layered structures, in which the three-partial LTW3 can exist. That can give an additional interest in the study of the SSZTW3 due to a possibility to use them along with LTW3 in different MEMS structures for further device microminiaturization. The LTW3 V_g-investigations were carried out in Ref. 18. The same investigations can be readily followed for the V_g of the SSZTW3 first type discussing about possible applications. It is thought that technical device realization of evaluating higher derivatives of the V_{ph} and V_g is needed concerning sensor application, because their changes with increase in the value of kh are several orders greater than any changes of the $V_{ph}(kh)$ and $V_g(kh)$. Indeed, the derivatives for each mode can be used in multi-functional technical devices, because it was recently suggested to use many modes in such devices operating their individual reactions, for example, to selected chemical elements. It is thought that technical

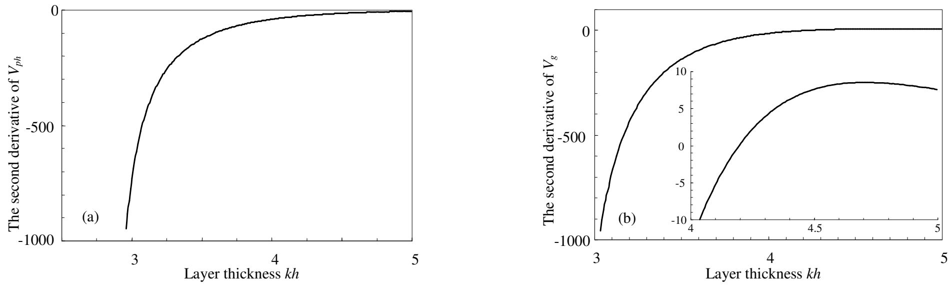

Fig. 8. The second derivatives of the phase (a) and group (b) velocities for the Au/ftorapatite structure. The insertion shows sign changing of the second derivative of group velocity.

devices, in which the derivatives are evaluated, will have a bigger sensitivity to smaller amount of chemical elements.

The second derivatives of the V_{ph} and V_g are shown in Figs. 8(a) and 8(b), respectively. The second derivative of the V_g can be readily calculated with the following formula taken from Ref. 30:

$$\frac{d^2V_g}{d(kh)^2} = 3\frac{d^2V_{ph}}{d(kh)^2} + (k - k_0)h\frac{d^3V_{ph}}{d(kh)^3}\,, \tag{31}$$

which represents the function from the second and third derivatives of the V_{ph} given in the appendix formulas (A6) and (A10), respectively. The $d^2V_{ph}/d(kh)^2$ was calculated with the appendix formula (A6), for which the dV_{ph}/dkh should be first known. It is expected that the dV_{ph}/dkh and dV_g/dkh will approach some constant values for $kh \to k_0h$, using the free QP approach with the relationship $V_g = 2V_{ph}$. However, it is difficult to verify due to great values of the derivatives. Also, it is obvious that the value of dV_g/dkh will change its sign because the V_g has one maximum. Therefore, the second derivative $d^2V_{ph}/d(kh)^2$ will behave like the well-known δ-function that appears frequently studying different problems. The third derivative of the V_{ph} calculated with the appendix formula (A10) is shown in Fig. 9 for the Au/ftorapatite structure. Calculation of the third derivative of V_g is more complicated, for which it is necessary to obtain the fourth derivative of V_{ph}.

The obtained results of calculations of the first and second derivatives of the V_g can be useful for finding inflection points in dependence of the group delay time $\tau = \Sigma/V_g$ (Σ is a gone distance) on the value of kh. That can have application in technical devices, for instance, dispersive delay lines.[10] It is well known that around an inflection point the $\tau(kh)$ has a linear dependence, and to find the linearity (a robot managed by special software can do it) the following first derivative should be found:

$$\frac{d\tau}{dkh} = -\frac{\Sigma}{V_g^2}\frac{dV_g}{dkh}\,. \tag{32}$$

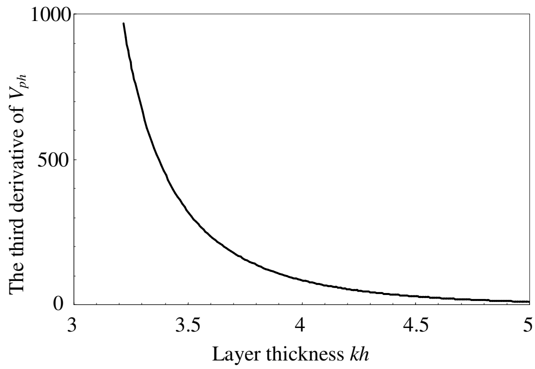

Fig. 9. The third derivative of the phase velocity V_{ph} for the Au/ftorapatite structure.

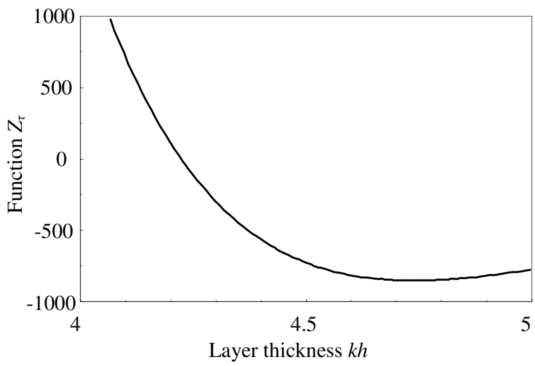

Fig. 10. Finding the inflection point for delay line application considering the Au/ftorapatite structure.

Hence, the $d^2\tau/d(kh)^2$ can be obtained from Eq. (32) and is defined by the following function[18]:

$$\frac{d^2\tau}{d(kh)^2} = 2\frac{\Sigma}{V_g^3}\left(\frac{dV_g}{dkh}\right)^2 - \frac{\Sigma}{V_g^2}\frac{d^2V_g}{d(kh)^2} = \frac{2\Sigma}{V_g^3}Z_r\,. \tag{33}$$

The functions V_g, dV_g/dkh, and $d^2V_g/d(kh)^2$ in Eqs. (32) and (33) are defined by formulas (23), (30), and (31), respectively. Therefore, at the inflection points the following condition should be fulfilled:

$$Z_r = \left(\frac{dV_g}{dkh}\right)^2 - \frac{V_g}{2}\frac{d^2V_g}{d(kh)^2} = 0\,. \tag{34}$$

The function Z_τ is shown in Fig. 10 for the SSZTW3 first type propagating in the Au/ftorapatite structure in the kh-range: $4.1 < kh < 5.0$. It is clearly seen in the figure that there is only a single inflection point at $kh \sim 4.21$. It is thought that also one inflection point can exist at $kh = k_0h$ for both the V_{ph} and V_g. However, it is very complicated to calculate the derivatives at $kh \to k_0h$.

It is noted that in many experiments the function $\tau(\omega)$ is used, but not the function $\tau(k)$. Therefore, it is necessary to follow investigations of the function $\tau(\omega)$ in the same way. Indeed, there are the following relationships between the derivatives $d\tau/dk$ and $d\tau/d\omega$ of the delay time τ as well as between dV_g/dk and $dV_g/d\omega$, using the definition $V_g = d\omega/dk$:

$$\frac{d\tau}{dkh} = V_g \frac{d\tau}{d\omega h} \quad \text{and} \quad \frac{1}{V_g^2}\frac{dV_g}{dkh} = \frac{1}{V_g}\frac{dV_g}{d\omega h}\,. \tag{35}$$

Hence, using the relationships in Eq. (35), it is possible to find dependence of the delay time τ on the nondimensional value of ωh or $k_{tm}h = \omega h/V_{tm}$, where h and V_{tm} are the material constant parameters described in the previous section. The function $\tau(\omega)$ is then written as follows:

$$\frac{d\tau}{d\omega h} = -\frac{\Sigma}{V_g^2}\frac{dV_g}{d\omega h}\,, \tag{36}$$

which becomes Eq. (32) by substituting the k instead of the ω. Similarly, substituting ω instead of k in Eq. (33) or applying differentiation to Eq. (36), the second derivative of the delay time τ is

$$\frac{d^2\tau}{d(\omega h)^2} = 2\frac{\Sigma}{V_g^3}\left(\frac{dV_g}{d\omega h}\right)^2 - \frac{\Sigma}{V_g^2}\frac{d^2V_g}{d(\omega h)^2}\,. \tag{37}$$

It is noted that calculating the derivatives $d\tau/d\omega h$ and $d^2\tau/d(\omega h)^2$ in (37) and (38) represents a more complicated problem, for which Ref. 18 can provide with the derivatives $dV_g/d\omega h$ and $d^2V_g/d(\omega h)^2$.

5. Conclusion

Theoretical investigations of SSZTW3 SAWs were presented in this paper studying layered systems, consisting of the thin film (Au) on different substrates listed in Table 1. These slow SAWs can propagate with the condition $\beta^L < \beta^S$ for the velocity equivalents β^L and β^S of the layer and substrate, respectively, using the condition for the material elastic constants: $C_{44}^L > C_{44}^S$. These slow SAWs possess the anti-plane polarization and single dispersive mode starting with zero V_{ph} at large values of kh and approaching the velocity V_{tm} at $kh \to \infty$. Some possible applications of the slow SAWs were discussed, which could be used in SAW filters and sensors similar to the lowest-order mode of Lamb-type waves (flexural plate waves). The V_{ph} and V_g were also calculated for the slow SAWs in different layered structures listed in Table 2. Also, the first and second derivatives of the velocities for the Au/ftorapatite structure possessing the slowest velocity $V_{tm} \sim 210$ m/s were calculated. The third derivative of the V_{ph} was also obtained. It is thought that the derivatives can be used to increase sensor sensitivity to small amount of chemical elements as a particular application. Also, the effective mass was evaluated and discussed for the case of zero V_{ph}, where both the V_{ph} and V_g show behavior of a free QP in vacuum. The evaluated QP masses for $h = 1$ μm are smaller than the mass of a free electron and depend on value of h. Note that this study can be useful for further investigations of slow waves in piezoelectric (piezomagnetic) layered systems as well as accounting different optic effects such as electro-optic and acousto-optic effects, see Ref. 35.

Acknowledgments

The author thanks the referees for their useful notes.

Appendix A

The derivatives obtained using the Leibniz formulae: $d(f(x)g(x))/dx$ and $d(f(x)g^{-1}(x))/dx$. Note that the V_{ph} derivatives of the SSZTW3 first type differ from those of the LTWs from Ref. 18.

The $d^2(\chi_3 h)/d(\zeta_3 h)^2$ represents the following function of the $\zeta_3 h$ using Eq. (19):

$$\frac{d^2\chi_3 h}{d(\zeta_3 h)^2} = \frac{2a}{\cosh^2(\zeta_3 h)}[\zeta_3 h \tanh(\zeta_3 h) - 1]\,. \tag{A1}$$

The third derivative $d^3(\chi_3 h)/d(\zeta_3 h)^3$ is obtained using formula (A1) as follows:

$$\frac{d^3\chi_3 h}{d(\zeta_3 h)^3} = \frac{2a\tanh(\zeta_3 h)}{\cosh^2(\zeta_3 h)}[3 - 2\zeta_3 h \tanh(\zeta_3 h)] + \frac{2a\zeta_3 h}{\cosh^4(\zeta_3 h)}\,. \tag{A2}$$

The first derivatives of the functions $\omega h(\zeta_3 h)$ and $kh(\zeta_3 h)$ are given by the following formulae, using Eqs. (12) and (13):

$$\frac{d\omega h}{d\zeta_3 h} = \left(\frac{\beta^L}{\alpha_f^S b}\right)^2 \frac{1}{\omega h(\zeta_3 h)}\left[-\zeta_3 h\left(\frac{\alpha_f^s}{\alpha_f^L}\right)^2 + \chi_3 h\frac{d\chi_3 h}{d\zeta_3 h}\right], \tag{A3}$$

$$\frac{dkh}{d\zeta_3 h} = \left(\frac{1}{\alpha_f^S b}\right)^2 \frac{1}{kh(\zeta_3 h)}\left[-\zeta_3 h\left(\frac{V_{t4}^L}{V_{t4}^S}\right)^2 + \chi_3 h\frac{d\chi_3 h}{d\zeta_3 h}\right]. \tag{A4}$$

Using the known first derivatives in Eqs. (A3) and (A4), it is possible to numerically calculate the dV_{ph}/dkh:

$$\frac{dV_{ph}}{dkh} = \frac{dV_{ph}}{d\zeta_3 h}\frac{d\zeta_3 h}{dkh} \quad \text{with} \quad \frac{dV_{ph}}{d\zeta_3 h} = \frac{1}{kh}\left(\frac{d\omega h}{d\zeta_3 h} - V_{ph}\frac{dkh}{d\zeta_3 h}\right). \tag{A5}$$

Further, the second derivative of the V_{ph} is equal to the following expression:

$$\frac{d^2V_{ph}}{d(kh)^2} = \frac{d}{d\zeta_3 h}\left(\frac{dV_{ph}}{dkh}\right)\frac{d\zeta_3 h}{dkh} = \left(\frac{dkh}{d\zeta_3 h}\right)^{-2}\left[\frac{d^2V_{ph}}{d(\zeta_3 h)^2} - \frac{d^2kh}{d(\zeta_3 h)^2}\frac{dV_{ph}}{dkh}\right], \tag{A6}$$

where the following second derivative is defined as follows:

$$\frac{d^2V_{ph}}{d(\zeta_3 h)^2} = \frac{1}{kh}\left(\frac{d^2\omega h}{d(\zeta_3 h)^2} - 2\frac{dkh}{d\zeta_3 h}\frac{dV_{ph}}{d\zeta_3 h} - V_{ph}\frac{d^2kh}{d(\zeta_3 h)^2}\right). \tag{A7}$$

In Eqs. (A6) and (A7), the second derivatives of the ωh and kh are given as follows:

$$\frac{d^2\omega h}{d(\zeta_3 h)^2} = -\frac{1}{\omega h}\left\{\left(\frac{d\omega h}{d\zeta_3 h}\right)^2 - \left(\frac{\beta^L}{\alpha_f^S b}\right)^2\left[-\left(\frac{\alpha_f^S}{\alpha_f^L}\right)^2 + \left(\frac{d\chi_3 h}{d\zeta_3 h}\right)^2 + \chi_3 h\frac{d^2\chi_3 h}{d(\zeta_3 h)^2}\right]\right\}, \tag{A8}$$

$$\frac{d^2kh}{d(\zeta_3h)^2} = -\frac{1}{kh}\left\{\left(\frac{dkh}{d\zeta_3h}\right)^2 - \left(\frac{1}{\alpha_f^S b}\right)^2\left[-\left(\frac{V_{t4}^L}{V_{t4}^S}\right)^2 + \left(\frac{d\chi_3h}{d\zeta_3h}\right)^2 + \chi_3h\frac{d^2\chi_3h}{d(\zeta_3h)^2}\right]\right\}. \tag{A9}$$

In Eqs. (A8) and (A9), the second derivative of the substrate damping wave number χ_3h with respect to the layer wave number ζ_3h is found using Eq. (A1).

The more complicated expression for the third derivative of the V_{ph} is given as follows:

$$\begin{aligned}\frac{d^3V_{ph}}{d(kh)^3} &= \frac{d}{d\zeta_3h}\left(\frac{d^2V_{ph}}{d(kh)^2}\right)\frac{d\zeta_3h}{dkh}\\ &= \left(\frac{dkh}{d\zeta_3h}\right)^{-3}\left[\frac{d^3V_{ph}}{d(\zeta_3h)^3} - 3\frac{dkh}{d\zeta_3h}\frac{d^2kh}{d(\zeta_3h)^2}\frac{d^2V_{ph}}{d(kh)^2} - \frac{d^3kh}{d(\zeta_3h)^3}\frac{dV_{ph}}{dkh}\right] \end{aligned} \tag{A10}$$

with the following third derivative of the phase velocity

$$\frac{d^3V_{ph}}{d(\zeta_3h)^3} = \frac{1}{kh}\left(\frac{d^3\omega h}{d(\zeta_3h)^3} - 3\frac{d^2kh}{d(\zeta_3h)^2}\frac{dV_{ph}}{d\zeta_3h} - 3\frac{dkh}{d\zeta_3h}\frac{d^2V_{ph}}{d(\zeta_3h)^3} - V_{ph}\frac{d^3kh}{d(\zeta_3h)^3}\right), \tag{A11}$$

where the following third derivatives of the frequency ωh and wave number kh are defined as follows:

$$\frac{d^3\omega h}{d(\zeta_3h)^3} = -\frac{1}{\omega h}\left\{3\frac{d\omega h}{d\zeta_3h}\frac{d^2\omega h}{d(\zeta_3h)^2} - \left(\frac{\beta^L}{\alpha_f^S b}\right)^2\left[3\frac{d\chi_3h}{d\zeta_3h}\frac{d^2\chi_3h}{d(\zeta_3h)^2} + \chi_3h\frac{d^3\chi_3h}{d(\zeta_3h)^3}\right]\right\}, \tag{A12}$$

$$\frac{d^3kh}{d(\zeta_3h)^3} = -\frac{1}{kh}\left\{3\frac{dkh}{d\zeta_3h}\frac{d^2kh}{d(\zeta_3h)^2} - \left(\frac{1}{\alpha_f^S b}\right)^2\left[3\frac{d\chi_3h}{d\zeta_3h}\frac{d^2\chi_3h}{d(\zeta_3h)^2} + \chi_3h\frac{d^3\chi_3h}{d(\zeta_3h)^3}\right]\right\}. \tag{A13}$$

In Eqs. (A12) and (A13), the third derivative $d^3(\chi_3h)/d(\zeta_3h)^3$ can be calculated using Eq. (A2).

References

1. A. E. H. Love, *Some problems of Geodynamics* (Cambridge University Press, London, England), p. 1911.
2. J. L. Bleustein, *Appl. Phys. Lett.* **13**, 412 (1968).
3. Yu. V. Gulyaev, *Sov. Phys. J. Exp. Theor. Phys. Lett.* **9**, 37 (1969).
4. Yu. V. Gulyaev and F. S. Hickernell, *Acoust. Phys. Rep.* **51**(1), 101 (2005) (in Russian).
5. A. A. Zakharenko, *J. Sound Vib.* **285** (4–5), 877 (2005).
6. M. I. Kaganov and I. L. Sklovskaya, *Sov. Phys. Solid State* **8**(12), 3480 (1966) (in Russian).
7. Yu. V. Gulyaev, *IEEE Trans. Ultrason. Ferroelectr. Freq. Contr.* **45**(4), 935 (1998).
8. M. Yamaguchi, *Jpn. J. Appl. Phys.* **42** (Part 1), 5B 2909 (2003).

9. H. Liu, Z. B. Kuang and Z. M. Cai, *Ultrasonics* **41**, 397 (2003).
10. E. Dieulesaint and D. Royer, *Elastic Waves in Solids: Applications to Signal Processing* translated by A. Bastin and M. Motz (English, J. Wiley, Chichester, New York, 1980), p. 511.
11. G. W. Farnell, Types and properties of surface acoustical waves, in *Acoustic Surface Waves*, Vol. 24, ed. A. A. Oliner (Springer Verlag, Berlin, Heidelberg, New York, 1978), pp. 26–109.
12. C. Lardat, C. Maerfeld and P. Tournois, *Proc. IEEE* **59**(3), 355 (1971).
13. G. W. Farnell and E. L. Adler, Elastic wave propagation in thin layers, in *Physical Acoustics*, Vol. 9, eds. W. P. Mason and R. N. Thurston (Academic Press, New York, 1972), pp. 35–127.
14. G. Kovacs and A. Venema, *Appl. Phys. Lett.* **61**(6), 639 (1992).
15. E. Gizeli, M. Liley, C. R. Lowe and H. Vogel, *Anal. Chem.* **69**, 4808 (1997).
16. M. Vellekoop and B. Jakoby, A Love-wave ice detector, in *Proc. IEEE Ultrasonic Symposium*, Vol. 1, 453 (1999).
17. J. Grate, S. Martine and Q. White, *Anal. Chem.* **65**(21), 940 (1993).
18. A. A. Zakharenko, *Nondestruct. Test. Eval.* **20**(4), 237 (2005).
19. G. G. Yaralioglu, M. H. Badi, A. S. Ergun, C. H. Cheng, B. T. Khuri-Yakub and F. L. Degertekin, *Appl. Phys. Lett.* **78**(1), 111 (2001).
20. A. Choujaa, N. Tirole, C. Bonjour, G. Martin, D. Hauden, P. Blind, A. Cachard and C. Pommier, *Sensor Actuat. A Phys.* **46**, 179 (1995).
21. A. Palma, L. Palmieri, G. Socino and E. Verona, *J. Appl. Phys.* **58**(8), 3265 (1985).
22. K. Toda, *J. Appl. Phys.* **44**(1), 56 (1973).
23. K. Toda, *J. Appl. Phys.* **45**(12), 5136 (1974).
24. T. Fujita and K. Toda, *Jpn. J. Appl. Phys.* **43**(8A), 5577 (2004).
25. X. Zhao, C. Kwan and K. M. Luk, Wireless nondestructive inspection of aircraft wing with ultrasonic guided waves, in *The 16th WCNDT 2004–World Conference on NDT, CD-ROM Proc.*, Internet Version of $\sim$ 600 Papers, 30 August–3 September 2004, Montreal, Canada.
26. B. A. Auld, *Acoustic Fields and Waves in solids* (Wiley, New York, 1973).
27. J. F. Nye, *Physical Properties of Crystals. Their Representation by Tensors and Matrices* (Clarendon Press, Oxford, 1989), p. 385.
28. A. A. Blistanov, V. S. Bondarenko, N. V. Perelomova, F. N. Strizhevskaya, V. V. Chkalova and M. P. Shaskol'skaya, Acoustical crystals, in *Acoustical Crystals*, ed. M. P. Shaskol'skaya (Nauka, Moscow, 1982), p. 632 (in Russian).
29. K. S. Aleksandrov and G. T. Prodaivoda, *Anisotropy of Elastic Properties of both Minerals and Rocks* (Publishing SB RAS, Novosibirsk, 2000), p. 354 (in Russian).
30. A. A. Zakharenko, *Acta Acust. United Acust.* **91**(4), 708 (2005).
31. I. A. Kaibichev and V. G. Shavrov, *Acoust. Phys. Rep.* **39**(5), 848 (1993) (in Russian).
32. Yu. V. Gulyaev and V. P. Plessky, *Sov. Pis'ma v Zhurnal Technicheskoi Phiziki* **3**(5), 220 (1977) (in Russian).
33. I. A. Viktorov, V. N. Kudryavtsev, V. G. Mozhaev and P. A. Pyatakov, *Sov. Akustich. Zhurnal* **28**(2), 164 (1982) (in Russian).
34. I. A. Viktorov, *Sov. Akustich. Zhurnal* **24**(5), 780 (1978) (in Russian).
35. V. P. Kamenov, Y. Hu, E. Shamonina, K. H. Ringhofer and V. Ya. Gayvoronsky, *Phys. Rev. E* **62**(2), 2863 (2000).